IOPscience iopscience.iop.org

Home Search Collections Journals About Contact us My IOPscience

Optimization of atomic Faraday filters in the presence of homogeneous line broadening

This content has been downloaded from IOPscience. Please scroll down to see the full text.

2015 J. Phys. B: At. Mol. Opt. Phys. 48 185001

(http://iopscience.iop.org/0953-4075/48/18/185001)

View the table of contents for this issue, or go to the journal homepage for more

Download details:

IP Address: 129.234.252.65
This content was downloaded on 23/09/2015 at 10:33

Please note that terms and conditions apply.

OPEN ACCESS
IOP Publishing
Journal of Physics B: Atomic, Molecular and Optical Physics
J. Phys. B: At. Mol. Opt. Phys. **48** (2015) 185001 (9pp)
doi:10.1088/0953-4075/48/18/185001

Optimization of atomic Faraday filters in the presence of homogeneous line broadening

Mark A Zentile, James Keaveney, Renju S Mathew, Daniel J Whiting, Charles S Adams and Ifan G Hughes

Joint Quantum Centre (JQC) Durham-Newcastle, Department of Physics, Durham University, South Road, Durham DH1 3LE, UK

E-mail: james.keaveney@durham.ac.uk

Received 15 April 2015, revised 22 June 2015
Accepted for publication 8 July 2015
Published 11 August 2015

Abstract

We show that homogeneous line broadening drastically affects the performance of atomic Faraday filters. We study the effects of cell length and find that the behaviour of 'line-centre' filters are quite different from 'wing-type' filters, where the effect of self-broadening is found to be particularly important. We use a computer optimization algorithm to find the best magnetic field and temperature for Faraday filters with a range of cell lengths, and experimentally realize one particular example using a micro-fabricated ^{87}Rb vapour cell. We find excellent agreement between our theoretical model and experimental data.

Keywords: FADOF, Faraday effect, wavelength filtering, atomic spectroscopy, Faraday filter, optimization

(Some figures may appear in colour only in the online journal)

1. Introduction

Devices utilizing thermal atomic vapour cells are of increasing interest since they offer high precision with a compact and relatively simple apparatus. Examples of atomic vapour cell devices include magnetometers [1, 2], gyroscopes [3, 4], clocks [5, 6], electric field sensors [7], microwave detectors [8, 9] and cameras [10–12], quantum memories [13–15], optical isolators [16], laser frequency references [17] and narrowband optical notch [18, 19] and bandpass filters [20, 21].

Making these devices more compact, power efficient and lighter is currently a burgeoning area of research [22–24], since it allows them to become practical consumer products. Particularly for devices that require an applied magnetic field, compact vapour cells [25–31] offer the additional advantage that small permanent magnets can be used to create a uniform magnetic field across the vapour cell [32], while consuming no power. Cells with a shorter path length require the medium to be heated more to increase the atomic number density. Not only will this increased heating cause more Doppler broadening but the increased number density will mean that self-broadening [33, 34] must be taken into account. Often these compact cells are produced with inert buffer gases, which are useful in many applications [26, 35, 36], but also contribute to line-broadening. In this article we investigate the effects of these broadening mechanisms on the performance of Faraday filters. When the cell dimensions reduce to the order of 1 μm, i.e. comparable to the transition wavelength, additional effects need to be taken into account which substantially change the form of the atomic susceptibility. These include atom-surface interactions [37, 38], Dicke narrowing [39, 40] and etalon effects [41]. Quantitative spectroscopy is still possible [38, 40, 42, 43] but the changes from a bulk cell are non-trivial. For this reason we limit the range of our investigation to cell lengths $\geqslant$100 μm.

Faraday filters were proposed in 1956 by Öhman [20] for astrophysical observations. They were later applied to solar observations [44, 45] and used to frequency stabilize dye lasers [46–48]. In the early 1990s the subject of Faraday filters was revived [49, 50]. Such filters have received increasing attention ever since, owing to their high performance in many applications. Faraday filters now find use in

Content from this work may be used under the terms of the Creative Commons Attribution 3.0 licence. Any further distribution of this work must maintain attribution to the author(s) and the title of the work, journal citation and DOI.

 © 2015 IOP Publishing Ltd Printed in the UK

remote temperature sensing [51], atmospheric lidar [52–55], diode laser frequency stabilization [56–58], Doppler velocimetry [45, 59, 60], communications [61] and quantum key distribution in free space [62], optical limitation [63], filtering Raman light [64], and quantum optics experiments [65, 66].

The Faraday filter spectrum is sensitive to many experimental parameters and so a theoretical model is useful for designing filters. Due to advances in computer hardware, it has only recently become practical (i.e. can be run on a desktop computer) to run optimization algorithms for these filters [67, 68]. In this paper we use computer optimization to find the best working conditions for compact Faraday filters. We find that homogeneous line broadening from buffer gas or self-broadening has a drastic effect on the performance of such filters. By incorporating line broadening effects into the theoretical model and optimizing temperature and magnetic field for a given cell length, one can partially mitigate the deleterious effect of line broadening. Until now, theoretical treatments of Faraday filters [69–71] have not included the effect of self-broadening. The homogeneous broadening mechanism of self-broadening is particularly important to include since it is unavoidable at high atomic densities, which are required when using very short cells. The structure of the rest of the article is as follows: in section 2 we introduce the typical experimental arrangement for Faraday filters and qualitatively explain how they work. In section 3 we introduce line centre and wing-type filters and explain their differences. In section 4 we introduce the computer optimization technique used to find the best working parameters and show the effect homogeneous broadening has on filter performance. Section 5 describes an experiment performed to compare with the theoretical optimizations. The results show that buffer-gas broadening and isotopic purity strongly affect the filter spectrum. Finally we draw our conclusions in section 6.

2. Theory and background

An atomic Faraday filter is formed by surrounding an atomic vapour cell with crossed polarizers (see figure 1). When an axial magnetic field (B) is applied across the cell, the medium becomes circularly birefringent causing the plane of polarization to rotate as light traverses the cell (the Faraday effect [72]), which leads to some transmission through the second polarizer. For a dilute atomic medium the effect is negligibly small except near resonances, and since atomic resonances are extremely narrow, this results in a narrowband filter. If the signal being detected is unpolarized then half of the light will not pass through the first polarizer. This limits the filter transmission to 50%. However using a polarizing beam splitter allows one to arrange two Faraday filters to allow each polarization component through with little loss [53].

In a similar way, if the magnetic field is perpendicular to the light propagation direction, one can also make a 'Voigt filter' [73] which exploits the Voigt effect [74]. However, in this paper we will only consider Faraday filters. We have chosen to consider the D_2 ($n^2S_{1/2} \rightarrow n^2P_{3/2}$) lines of potassium and rubidium where n= 4 or 5 respectively.

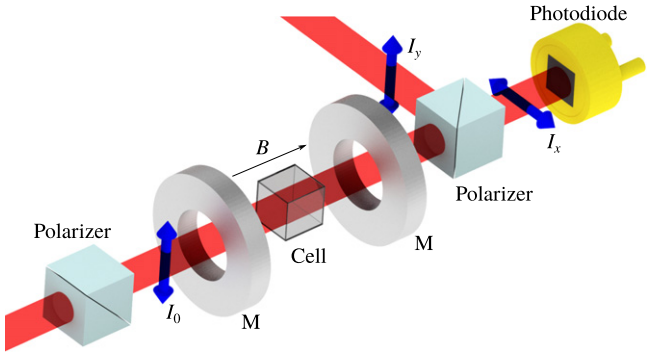

Figure 1. Illustration of the experimental arrangement. A microfabricated $1 \times 1 \times 1$ mm^3 ^{87}Rb vapour cell is placed between two axially magnetized ring magnets. This arrangement is then placed between two crossed polarizers, forming the filter. The filter is tested by monitoring transmission of a laser beam with a photodiode. The filter transmission is defined as the intensity of light transmitted through the second polarizer (I_x) divided by the initial intensity before the cell (I_0). Light out of the passband frequency is either scattered in the cell or rejected at the second polarizer (I_y).

For a given cell length the parameters that affect the Faraday filter transmission spectra are the applied magnetic field (B) and cell temperature (T). The effect of T is predominantly to change the atomic number density [75] and secondly the Doppler width, while B causes circular birefringence and dichroism. In general the filter spectrum is a complicated function of these two parameters, due to the large number of non-degenerate Zeeman-shifted transitions, each with different transition strengths and partially overlapping lineshape profiles. However, it is possible to accurately compute the filter profile with a computer program [67, 71, 76].

We use the ElecSus program to calculate the filter spectrum. The full description of how the program works can be found in [76]; here we summarize the key points. An atomic Hamiltonian is built up from contributions from hyperfine and magnetic interactions. The eigenvalues allow the transition frequencies to be calculated while the eigenstates are used to calculate their strengths. The electric susceptibility is then calculated by adding the appropriate (complex) line-shape at each transition frequency, scaled by its strength. The real part of the electric susceptibility can be used to calculate dispersion, while the imaginary part can be used to calculate extinction [78]. The imaginary part of these line-shapes have a Voigt profile [77], which is a convolution between inhomogeneous broadening (Gaussian profile from Doppler broadening) and homogeneous broadening (Lorentzian profile). Typically, the full-width half maximum of the homogeneous linewidth sums contributions from natural broadening (Γ_0), self-broadening (Γ_{self}) and buffer gases (Γ_{buf}). Any source of homogeneous broadening affects the line shape in the same way, i.e. to increase the Lorentzian component of the line width. In this sense, the exact source of broadening is unimportant. Calculating the lineshape allows for prediction of a variety of experimental spectra, of which the Faraday filter spectrum is one. The result is given as a function of detuning $\Delta/2\pi \equiv (\omega - \omega_0)/2\pi$, where ω is the angular

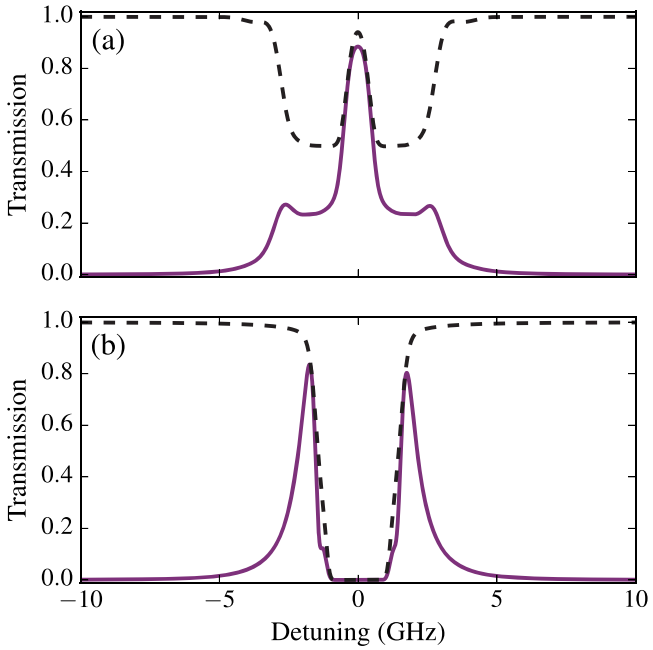

Figure 2. A comparison of (a) line-centre and (b) wing-type Faraday filters. For line-centre filters, the peak filter transmission occurs at the unshifted resonance frequency, whereas for wing-type filters, the peak transmission occurs either side of the unshifted resonance line. Here we simulate a natural abundance K vapour with $L = 2$ mm. In panel (a) the temperature $T = 110$ °C and applied field $B = 900$ G, whereas in panel (b) $T = 150$ °C and $B = 100$ G. The solid lines show the filter transmission $\mathcal{T}_x$, whereas the dashed lines show total cell transmission $\mathcal{T}_x + \mathcal{T}_y$, equivalent to removing the polarizer between the cell and photodiode.

frequency of the laser light and ω_0 is the global (weighted across all transitions) line-centre angular frequency.

3. Line-centre and wing-type Faraday filters

Atomic Faraday filters can be broadly divided into two types —line-centre and wing-type—depending on where the peak transmission lies with respect to the atomic resonances. As we shall show in subsequent analysis, their relative sensitivity to line broadening is quite different. In this section we give an overview of the two filter types.

As their name suggests, line-centre filters have their peak transmission at or near to the centre of the unshifted (in the absence of magnetic field) atomic resonance line(s). Wing-type filters typically have very little transmission on resonance, but have two transmission peaks to either side of the unshifted atomic resonance. In figure 2 we compare theoretically the two filter types, for the case of potassium. We stress that these are not optimal filters, merely examples to show the two filter types clearly. Because the hyperfine structure is completely masked by Doppler broadening, the potassium filters present the cleanest example of atomic Faraday filtering in alkali-metal atoms, close to the simplest case of a $J = 0$ to $J = 1$ transition. In addition, both line-centre (panel (a)) and wing-type (panel (b)) filters are demonstrable with moderate applied fields of 900 G and 100 G, respectively. This is in contrast to Rb where the complex hyperfine structure and isotopic abundance ratios make finding a line-centre filter difficult, and the resulting spectrum is complex (see figure A1 in the appendix).

The filter peaks are found in regions where the light is rotated by close to $\pi/2$, without significant absorption. The rotation occurs through circular birefringence, and can be obtained in two ways. One way is to have a large magnetic field, such that the absorption lines are significantly split by the magnetic field. This produces a large relative birefringence between the two circular polarization components, so the atomic density can be relatively low to achieve a $\pi/2$ rotation. This is the usual case for producing line-centre filters, as shown in panel (a) of figure 2. In contrast, one can use much lower magnetic fields, with a concomitantly higher density. In this case there is less Zeeman splitting and hence less relative birefringence, but the density compensates for this to produce an absolute birefringence that causes $\pi/2$ rotation. In addition to the rotation, the large density also causes a large resonant absorption, so the filter transmission peak occurs in the wings, as shown in panel (b).

4. Optimization

4.1. Figure-of-merit choices

The signal-to-noise ratio of a narrowband signal in broadband noise is greatly improved by using a bandpass filter. For the case of white noise, the noise power is directly proportional to the bandwidth of a top-hat filter. For a more general filter profile, the equivalent-noise bandwidth (ENBW) is a quantity which is inversely proportional to the signal to noise ratio, and is defined as

$$\mathrm{ENBW} = \frac{\int_0^\infty \mathcal{T}_x(\nu)\mathrm{d}\nu}{\mathcal{T}_x(\nu_s)}, \tag{1}$$

where $\mathcal{T}_x = I_x/I_0$ is the transmitted light intensity after the filter relative to the input intensity, ν is the optical frequency and ν_s is the signal frequency. If there is freedom in the exact position of the signal frequency we can set it to the frequency which gives the maximum transmission ($\mathcal{T}_x(\nu_s) = \mathcal{T}_{\max}$).

Although minimizing the ENBW is desirable, this usually comes with a reduction in transmission [67]. Using the following figure of merit,

$$\mathrm{FOM} = \frac{\mathcal{T}_{\max}^2}{\int_0^\infty \mathcal{T}_x(\nu)\mathrm{d}\nu} = \left.\frac{\mathcal{T}_{\max}}{\mathrm{ENBW}}\right|_{\mathcal{T}_x(\nu_s)=\mathcal{T}_{\max}}, \tag{2}$$

we can maintain a reasonably large transmission [67], while minimizing the ENBW.

Alternately, one may need to optimize filter performance for a specific frequency. In this case, we use the following

figure of merit,

$$\mathrm{FOM}' = \left.\frac{\mathcal{T}_x^2(\nu_s)}{\int_0^\infty \mathcal{T}_x(\nu)\mathrm{d}\nu}\right|_{\nu_s=\omega_0/2\pi}, \qquad (3)$$

where we set ν_s to be the frequency of interest.

To calculate these figures-of-merit we simulate filter spectra with a range of 60 GHz around the atomic weighted line-centre with a 10 MHz grid spacing. The integration is performed by a simple rectangle method. The limitation to the accuracy of the calculated figures-of-merit comes from the grid spacing; a finer grid spacing of 1 MHz only improves the accuracy by 0.2%.

4.2. Constant $\mathcal{N}L$ optimization

The optical signal in a vapour cell device comes from the interaction of the light with all the atoms in the beam path. This means that for compact vapour cells with shorter path lengths, the atomic number density must increase to compensate for the loss of optical depth. For example the Faraday filter spectrum can be thought of as some function of the product $\sigma\mathcal{N}L$, where $\mathcal{N}$ is the number density, L is the length of the medium and σ is the cross-section for light scattering with a single atom. Assuming σ remains constant, we can achieve the same filter when reducing L by increasing $\mathcal{N}$ by the same factor. Therefore, once good parameters of B and T are found for a particular cell length, we can find new appropriate parameters by changing the temperature such that $\mathcal{N}L$ remains constant. However, this simple argument breaks down at some point since σ is not generally constant. At high densities, interactions between atoms cause self-broadening, which can be modelled as $\Gamma_{\mathrm{self}} = \beta\mathcal{N}$, where β is the self-broadening parameter [34]. In addition, by increasing the cell temperature we also change the amount of Doppler broadening. Both Doppler and self-broadening affect σ. To find where these effects become important we need to compare it with a computer optimization technique, which can find the best parameters at each cell length.

4.3. Computerized optimization procedure

Efficiently finding the optimal experimental conditions for a Faraday filter requires three elements. First, a computer program is needed which can calculate the spectrum with the experimental conditions as parameters. Secondly, a definition of a figure of merit, or conversely a 'cost function' [79], to numerically quantify which filter spectra are more desirable. The figures-of-merit used in this work were described in section 4.1. Finally, the chosen figure of merit is then maximized (or the cost function is minimized) by varying the parameters according to some algorithm. We used a global minimization technique [80] which includes the random-restart hill climbing meta-algorithm [79] in conjunction with the downhill simplex method [81] to find the values of B and T which maximized our figures of merit. This routine was used in conjunction with the ElecSus program [76] which calculated the filter spectra. ElecSus was used because it includes the effect of self-broadening, which is essential for this study, and also because it evaluates the filter spectrum quickly (<1 s) which makes this kind of optimization practical (i.e. results can be obtained in under an hour), since the filter spectra need to be evaluated a few thousand times.

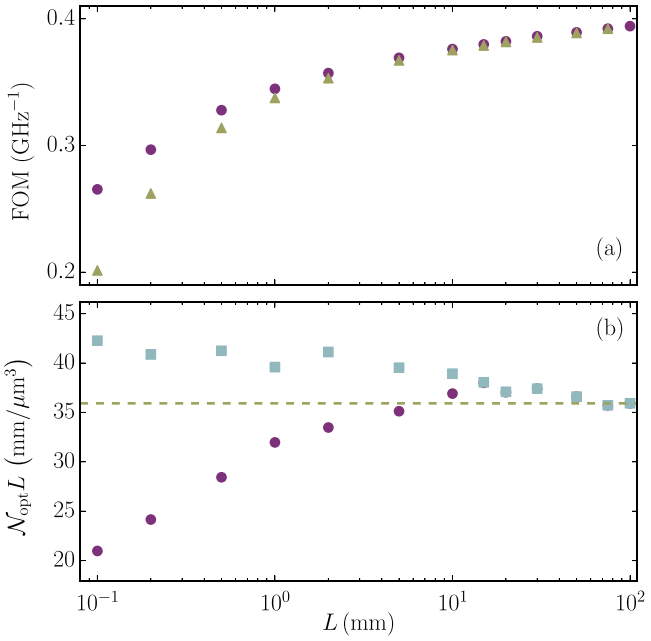

Figure 3. Filter performance as cell length is changed, for a wing-type ^{87}Rb filter near the D_2 resonance lines. (a) The olive triangles show the figure of merit found by taking the optimal magnetic field and temperature of the 100 mm length cell and changing the temperature such that $\mathcal{N}L = \mathrm{const}$. The purple circles show the figure of merit maximized by optimizing the magnetic field and temperature for each cell length. (b) Atomic number density after optimization, ($\mathcal{N}_{\mathrm{opt}}$), multiplied by cell length (L). The purple circles show the results when self-broadening is included in the model for the filter spectrum, while the light blue squares show the result without self-broadening.

4.4. Optimization while reducing cell length

Since much of the motivation behind this work deals with decreasing the size of vapour cells for use in applications, it is prudent to investigate how filter performance changes with cell thickness.

In figure 3 we show filter optimization as a function of cell length for a wing-type filter. In panel (a), the figure of merit of equation (2) was maximized while simulating an isotopically pure ^{87}Rb vapour with $L = 100$ mm, finding the optimal values of B and T to be 67.3 G and 60.9 °C respectively. We assumed a constant $\mathcal{N}L$-product (section 4.2) to estimate the new values of the vapour cell temperature for a range of shorter cell lengths, and then evaluated the figures-of-merit (olive triangles). In addition, the figures-of-merit were re-optimized (section 4.3) for each cell length (purple spots). The figure of merit changes with cell length, as is expected, since the decrease in length must be compensated by an increase in density. For long cells the re-optimization

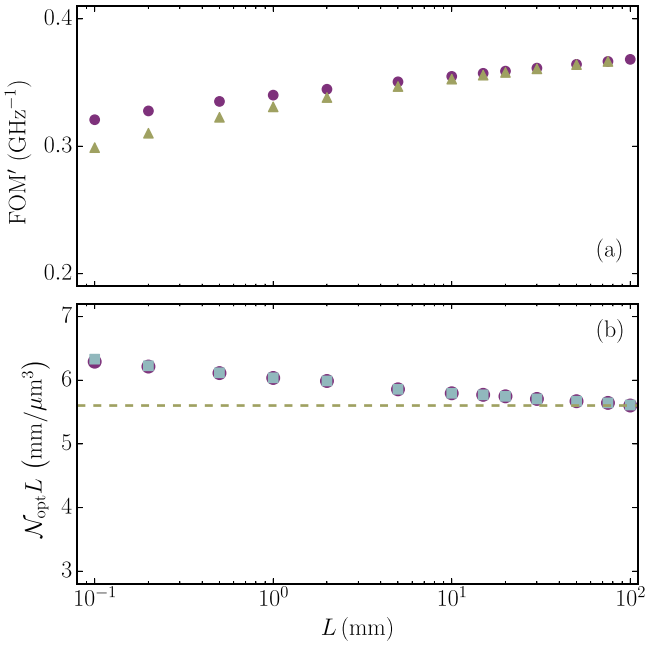

Figure 4. Filter performance as cell length is changed, for a line-centre natural abundance K filter near the D_2 resonance lines. All symbols are the same as for figure 3. In addition, the relative scaling of panel (b) is equivalent to figure 3(b).

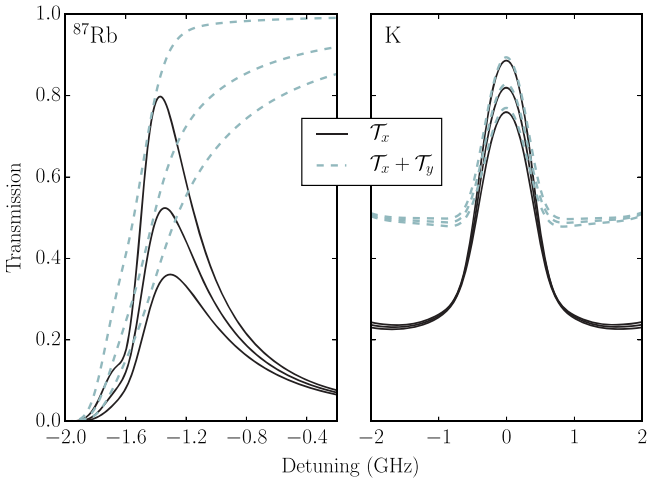

Figure 5. Filter transmission (I_x/I_0, solid black curve) and cell transmission ($(I_x + I_y)/I_0$, dashed blue curve) as a function of detuning ($\Delta/2\pi$), zoomed around the region of peak transmission. The left panel models a ^{87}Rb vapour on the D_2 line, while the right panel models the ^{39}K D_2 line; both of length 1 mm. The cell parameters were set to $B = 85.8$ G and $T = 127.8$ °C ($\mathcal{N} = 3.2 \times 10^{13}$ cm^{-3}) for ^{87}Rb, and $B = 864$ G and $T = 136.1$ °C ($\mathcal{N} = 6.0 \times 10^{12}$ cm^{-3}) for K. The uppermost lines were calculated with a Lorentzian width given by natural broadening only (∼6 MHz) while the middle and lower lines have a further 50 and 100 MHz of Lorentzian width. The global line-centres occur at 384.23042812 THz [82, 83] for the Rb D_2 line and 391.01617854 THz [84] for the K D_2 line.

has little effect, since self-broadening for these densities is small compared to the natural linewidth. As the cell thickness decreases, the density must rise to compensate, causing significant additional broadening which has a deleterious effect on the filter performance. Re-optimization can somewhat mitigate the decrease in performance (purple points in figure 3(a)), but there remains a smooth degradation in filter performance as the length decreases. However, as the cell thickness becomes comparable to the transition wavelength, or smaller, the physics changes significantly, as previously discussed in section 1.

In figure 3(b) we plot the optimum density-length product, $\mathcal{N}_{\rm opt}L$, with (purple circles) and without (blue squares) self-broadening included in the model. For cell lengths above ∼10 mm, and hence relatively low density, there is little effect, since self-broadening has a negligible effect at low densities. However, as cell thickness reduces below 10 mm, the difference becomes clear. The optimum conditions, including line broadening effects, are found by reducing $\mathcal{N}_{\rm opt}L$ (and hence reducing broadening). In other words, line broadening for wing-type filters has a significant impact on the performance of the filters.

In contrast to the wing-type filter, in figure 4 we show a similar analysis of the potassium line-centre filter. For these filters we find in panel (a) that the length dependence is much less severe than wing-type filters—the performance drops off much more slowly with decreasing cell length. In addition, re-optimization has a much smaller effect (both in terms of absolute and relative filter figure of merit), and when we compare re-optimization with and without self-broadening (panel (b)), we find very little difference in the optimized $\mathcal{N}_{\rm opt}L$-products. Hence self-broadening has a much smaller effect than for the wing-type filters. In the next section we explore the reasons for this behaviour.

4.5. Comparison of wing-type and line-centre filter performance with additional line broadening

The difference between wing-type and line-centre filters can be understood by inspection of the spectra. In figure 5 we show the filter peaks of a ^{87}Rb wing-type filter and a ^{39}K line-centre filter with varying levels of additional broadening. Increases in Lorentzian broadening cause a decrease in transmission through the vapour cell at the filter frequency. This effect is far more pronounced for the wing-type filters, as can be seen in figure 5, where adding 100 MHz of extra broadening to the wing-type filter causes the transmission peak to drop by more than a factor of 2. In contrast, the same additional 100 MHz added to a line-centre filter causes only a 15% (relative) drop in peak transmission. The homogeneous broadening has a large effect in the wings of the resonance. Here, the influence of the long-tailed Lorentzian lineshape is much more prominent than that of the Gaussian line shape from Doppler broadening [85]. A higher optical depth transition feature will show this effect more strongly. This is one of the differences between wing and line-centre type filters. Wing-type filters rely on the sharp decrease in transmission caused by the atomic resonances to create narrow filter transparencies. This means that the circular dichroism cannot be too large since both polarizations need be scattered in the cell to sharply reduce the filter transmission to zero. However, a small amount of dichroism means that there is a small

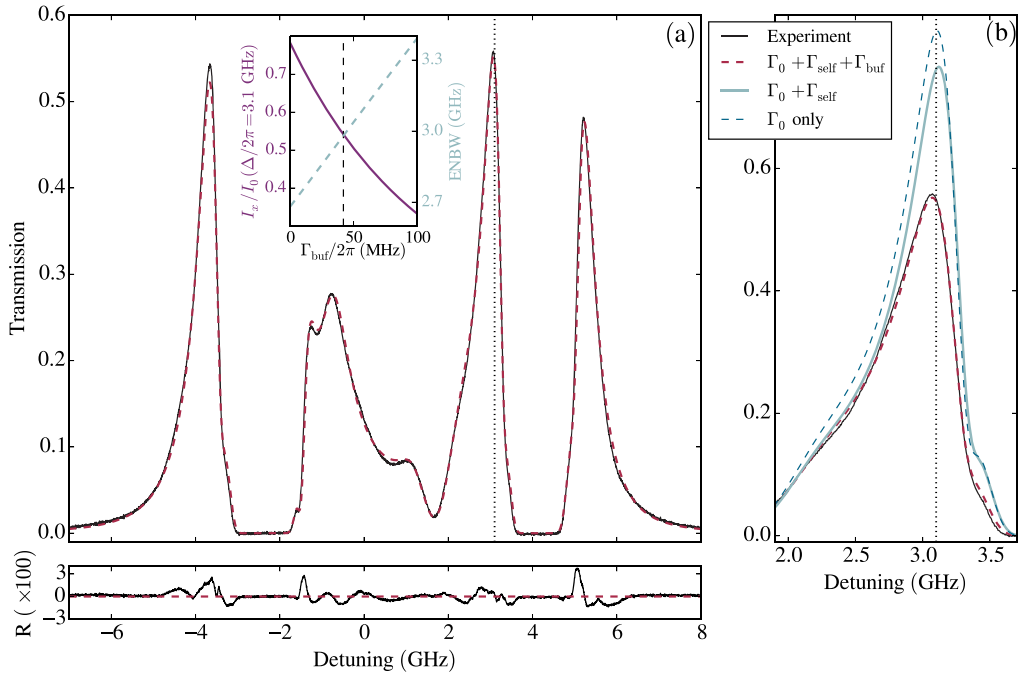

Figure 6. Experimental and theoretical Faraday-filter spectra on the rubidium D_2 line as a function of detuning ($\Delta/2\pi$) from the weighted line-centre. A 1 mm length vapour cell was used with an isotopic ratio of 99% ^{87}Rb to 1% ^{85}Rb. The solid black line in panel (a) shows the experimental filter spectrum and the dashed (red) line shows the fit to theory that includes the natural, self, and buffer gas induced (Γ_{buf}) Lorentzian broadening effects. Below panel (a) the residuals, R, (the difference between experiment and theory) are plotted. There is an RMS deviation between experiment and theory of 0.6%. The inset of panel (a) shows the effect of Γ_{buf} on transmission (solid purple line) and ENBW (dashed blue line) of theoretical filter spectra. The vertical dashed line marks the amount of buffer-gas broadening seen in the experiment. Panel (b) shows a zoomed in region around the peak at 3.1 GHz, including theoretical curves with only natural homogeneous broadening (Γ_0, dashed blue), and with natural and self-broadening ($\Gamma_0 + \Gamma_{self}$, solid blue).

relative birefringence, which means that a high number density is required to create the large absolute birefringence necessary for the rotation of $\pi/2$. Conversely, the line-centre filter operates in a region of the spectrum that exhibits large circular dichroism, such that the transitions which absorb each polarization of light are almost completely separated. We can see this in figure 2 where the cell is optically thick for just one circular polarization on either side of the transparency (causing ≈50% transmission of linearly polarized light through the cell and ≈25% transmission though the filter). This large dichroism comes with a large relative birefringence, meaning that the number density can be lower for a line-centre filter (and hence self-broadening is lower).

5. Experiment

To compare theory with experiment for a compact cell, we used a micro-fabricated $1 \times 1 \times 1$ mm^3 isotopically enriched ^{87}Rb cell [27]. The isotopic abundance of ^{85}Rb was found by transmission spectroscopy to be (1.00 ± 0.02)%, in a similar way to that demonstrated in [32]. The isotopic impurity affects the filter spectra, therefore the filter parameters were optimized taking this into account. We found the optimal parameters to be $B = 72.0$G and $T = 137.5\,^\circ$ C, which gave a transmission peak at a detuning of 3.1 GHz.

The experimental Faraday filter arrangement is illustrated in figure 1. The cell was placed in an oven and heated near the optimal temperature, while the applied axial magnetic field was produced using a pair of permanent ring magnets. The field inhomogeneity across the cell was less than 1%. Two crossed Glan–Taylor polarizers were placed around the cell to form the filter. A weak-probe [86, 87] beam from an external cavity diode laser was focussed using a lens (not shown in figure 1) with a 30 cm focal length to a $1/e^2$ diameter of 80 μm, and was sent through the filter such that the focus was approximately at the location of the cell. After the filter, the beam was focussed onto an amplified photodiode. The laser frequency was scanned across the Rb D_2 transition, and was calibrated using the technique described in [88].

Panel (a) of figure 6 shows the experimental filter spectrum plotted with a fit to theory using ElecSus [76]. The only fit parameters are temperature and magnetic field, and for figure 6 were found to be $B = 73$ G and $T = 138.5\,^\circ$ C. A further 42 MHz of Lorentzian broadening (Γ_{buf}) was added in addition to Γ_0 and Γ_{self}, due to the presence of a small quantity of background buffer gas in the vapour cell. This value was not fitted, but separately measured by transmission spectroscopy. Panel (b) of figure 6 shows the filter spectrum zoomed into the main peak. In addition to the experimental and theory fit is the filter spectrum for the optimization that did not include the buffer-gas broadening. We can see that the additional broadening drastically affects the filter transmission. Also by artificially removing the effect of self-

Table 1. Maximum transmission (T_{max}), equivalent-noise bandwidth (ENBW) and their ratio (FOM) for a 1 mm long isotopically enriched Rb vapour cell. The magnetic field and temperature were 73 G and 138.5 °C respectively. The first row represents the fit to the experiment shown in figure 6, while subsequent rows give the values after certain physical effects were removed (theoretically).

Spectrum	T_{max}	ENBW (GHz)	FOM (GHz^{-1})
Fit to experiment	0.55	3.0	0.18
No buffer gas	0.77	2.6	0.29
No self-broadening or buffer gas	0.83	2.6	0.31

broadening from the theory, we again see a larger transmission. Table 1 quantitatively compares the transmission, ENBW and figure of merit for the curves shown in figure 6. Due to the 1% ^{85}Rb impurity, the peak transmission occurs at $\Delta/2\pi = 3.1$ GHz rather than near -1.3 GHz if the cell were isotopically pure (see figure A1(b) in the appendix). This is due to the interplay between hyperfine energy spacings and the sensitivity of the Faraday rotation. At -1.3 GHz, the presence of the 1% ^{85}Rb impurity causes further rotation and absorption since this frequency is near to the ^{85}Rb absorption lines (unshifted detuning -1.4 GHz). For the peak at 3.1 GHz, the other ^{85}Rb absorption line is much further detuned (unshifted detuning 1.6 GHz) and hence does not significantly affect the Faraday filter peak. The inset of panel (a) shows the filter transmission at a detuning of 3.1 GHz and the ENBW as a function of Γ_{buf}. The transmission decreases while the ENBW increases, showing that the performance (as measured by the ratio transmission to ENBW) of this kind of Faraday filter deteriorates quickly with increasing buffer gas pressures.

The amount of broadening due to buffer gas pressure that we observe typically corresponds to approximately 1–2 Torr of buffer gas [89, 90]. The fact that this small pressure affects the filter spectra by a large amount shows that the wing-type Faraday filter spectra are very sensitive to buffer gas pressure. It has previously been shown that nonlinear Faraday rotation can be a sensitive probe of buffer gas pressure [91], being non-invasive and using a simple apparatus. Our results show that it may be possible to use the linear Faraday effect instead, for which it is easier to model the effect of buffer pressure. However, it is not yet clear if this is more sensitive than using transmission spectroscopy [92].

6. Conclusions

We have described an efficient computerized method to optimize the cell magnetic field and temperature for short cell length Faraday filters with additional homogeneous broadening from various sources. From theoretical spectra we see that wing-type filters in particular are significantly affected by homogeneous broadening, while line-centre filters are less sensitive. We performed an experiment to realize a wing-type filter using a micro-fabricated 1 mm length ^{87}Rb vapour cell, and find excellent agreement with theory. While buffer gases can enhance some signals using vapour cells [35], they should be kept to a minimum in order to achieve the narrowest Faraday filters with the highest transmission.

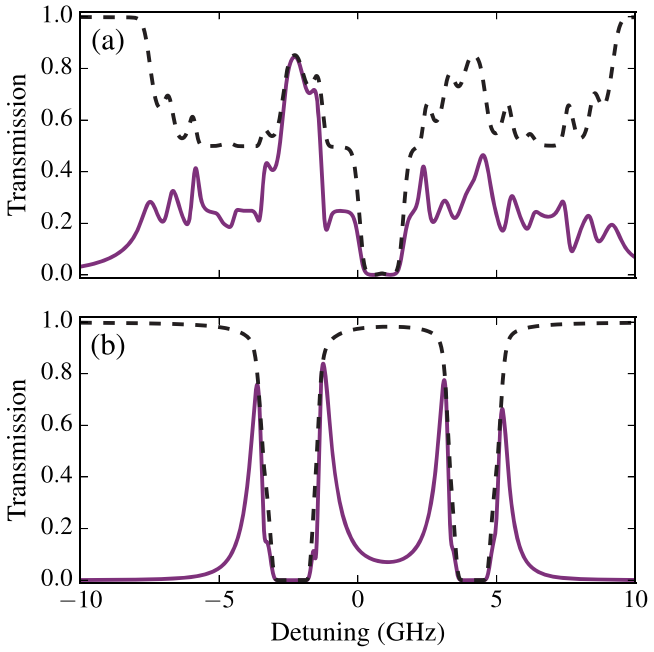

Figure A1. An equivalent analysis to figure 2 for a pure ^{87}Rb vapour. Panel (a) shows a line centre filter, panel (b) shows a wing-type filter. In contrast to potassium, the Rb line centre filter is much less clean due to the complex hyperfine structure. Because the transition strengths from the two hyperfine ground states are different, it is not possible to simultaneously have a useful filter (i.e. high transmission with rejection at other frequencies) at both of the unshifted detunings for the resonance groups from each ground state hyperfine level (-2.4 and 4.4 GHz). The model parameters are as follows: cell length $L = 1$ mm, (a) $T = 120$ ° C, $B = 1200$ G, (b) $T = 137.5$ ° C, $B = 72$ G (same as the experimental data of figure 6, but 100% ^{87}Rb instead of 99%).

Acknowledgments

We thank W J Hamlyn for his contribution to the experiment. We are grateful to S Knappe for providing the vapour cell used in the experiment. We acknowledge financial support from EPSRC (grant EP/L023024/1) and Durham University. RSM was funded by a BP Summer Research Internship. The data presented in this paper are available from http://dx.doi.org/10.15128/kk91fk598.

Appendix

Here we show a supporting figure which is a similar analysis to figure 2 for the case of a pure ^{87}Rb vapour. In contrast to potassium, the two hyperfine ground states are resolved leading to two distinct filter regions. The wing-type filter remains clean but, due to the complex hyperfine structure, the line-centre filter performance is poor, both in terms of the

maximum filter transmission and the broad transmission pedestal.

References

[1] Kominis I K, Kornack T W, Allred J C and Romalis M V 2003 *Nature* **422** 596
[2] Budker D and Romalis M 2007 *Nat. Phys.* **3** 227
[3] Lam L K, Phillips E, Kanegsberg and E and Kamin G W 1983 *SPIE Proc.* **412** 272
[4] Kornack T W, Ghosh R K and Romalis M V 2005 *Phys. Rev. Lett.* **95** 230801
[5] Knappe S, Shah V, Schwindt P D D, Hollberg L, Kitching J, Liew and L-A and Moreland J 2004 *Appl. Phys. Lett.* **85** 1460
[6] Camparo J 2007 *Phys. Today* **60** 33
[7] Mohapatra A K, Bason M G, Butscher B, Weatherill and K J and Adams C S 2008 *Nat. Phys.* **4** 890
[8] Sedlacek J A, Schwettmann A, Kübler H, Löw R, Pfau and T and Shaffer J P 2012 *Nat. Phys.* **8** 819
[9] Sedlacek J A, Schwettmann A, Kübler H and Shaffer J P 2013 *Phys. Rev. Lett.* **111** 063001
[10] Böhi P and Treutlein P 2012 *Appl. Phys. Lett.* **101** 181107
[11] Horsley A, Du G-X, Pellaton M, Affolderbach C, Mileti G and Treutlein P 2013 *Phys. Rev.* A **88** 063407
[12] Fan H Q, Kumar S, Daschner R, Kübler H and Shaffer J P 2014 *Opt. Lett.* **39** 3030
[13] Julsgaard B, Sherson J, Cirac J I, Fiuráusek J and Polzik E S 2004 *Nature* **432** 482
[14] Lvovsky A I, Sanders B C and Tittel W 2009 *Nat. Photonics* **3** 706
[15] Sprague M R, Michelberger P S, Champion T F M, England D G, Nunn J, Jin X-M, Kolthammer W S, Abdolvand A, Russell P St J and Walmsley I A 2014 *Nat. Photonics* **8** 287
[16] Weller L, Kleinbach K S, Zentile M A, Knappe S, Hughes I G and Adams C S 2012 *Opt. Lett.* **37** 3405
[17] Affolderbach C and Mileti G 2005 *Rev. Sci. Instrum.* **76** 073108
[18] Miles R B, Yalin A P, Tang Z, Zaidi S H and Forkey J N 2001 *Meas. Sci. Technol.* **12** 442
[19] Uhland D, Rendler T, Widmann M, Lee S-Y, Wrachtrup J and Gerhardt I 2015 arXiv:1502.07568v1
[20] Öhman Y 1956 *Stockholms Obs. Ann.* **19** 3
[21] Beckers J M 1970 *Appl. Opt.* **9** 595
[22] Mescher M J, Lutwak R and Varghese M 2005 *Solid-State Sensors, Actuators and Microsystems, 2005 Digest of Technical Papers 13th Int. Conf. on TRANSDUCERS '05*vol 1 pp 311–6
[23] DeNatale J F, Borwick R L, Tsai C, Stupar P A, Lin Y, Newgard R A, Berquist R W and Zhu M 2008 *Position Location and Navigation Symposium 2008 IEEE/ION* pp 67–70
[24] Mhaskar R, Knappe S and Kitching J 2012 *Appl. Phys. Lett.* **101** 241105
[25] Sarkisyan D, Bloch D, Papoyan A and Ducloy M 2001 *Opt. Commun.* **200** 201
[26] Liew L-A, Knappe S, Moreland J, Robinson H, Hollberg L and Kitching J 2004 *Appl. Phys. Lett.* **84** 2694
[27] Knappe S, Gerginov V, Schwindt P D D, Shah V, Robinson H G, Hollberg L and Kitching J 2005 *Opt. Lett.* **30** 2351
[28] Su J, Deng K, Wang Z and Guo D-Z 2009 *IEEE Int. Frequency Control Symp. 2009 Joint with the 22nd European Frequency and Time forum* pp 1016–8
[29] Baluktsian T, Urban C, Bublat T, Giessen H, Löw R and Pfau T 2010 *Opt. Lett.* **35** 1950
[30] Tsujimoto K, Ban K, Hirai Y, Sugano K, Tsuchiya T, Mizutani N and Tabata O 2013 *J. Micromech. Microeng.* **23** 115003
[31] Straessle R, Pellaton M, Affolderbach C, Pétremand Y, Briand D, Mileti G and de Rooij N F 2014 *Appl. Phys. Lett.* **105** 043502
[32] Weller L, Kleinbach K S, Zentile M A, Knappe S, Adams C S and Hughes I G 2012 *J. Phys. B: At. Mol. Opt. Phys.* **45** 215005
[33] Lewis E L 1980 *Phys. Rep.* **58** 1
[34] Weller L, Bettles R J, Siddons P, Adams C S and Hughes I G 2011 *J. Phys. B: At. Mol. Opt. Phys.* **44** 195006
[35] Brandt S, Nagel A, Wynands R and Meschede D 1997 *Phys. Rev.* A **56** R1063
[36] Vogl U and Weitz M 2009 *Nature* **461** 70
[37] Epple G, Kleinbach K S, Euser T G, Joly N Y, Pfau T, Russell P St J and Löw R 2014 *Nat. Commun.* **5** 4132
[38] Whittaker K A, Keaveney J, Hughes I G, Sargsyan A, Sarkisyan D and Adams C S 2014 *Phys. Rev. Lett.* **112** 253201
[39] Dicke R 1953 *Phys. Rev.* **89** 472
[40] Keaveney J, Sargsyan A, Krohn U, Hughes I G, Sarkisyan D and Adams C S 2012 *Phys. Rev. Lett.* **108** 173601
[41] Keaveney J 2013 Cooperative interactions in dense thermal Rb vapour confined in nm-scale cells *PhD Thesis* Durham
[42] Keaveney J, Hughes I G, Sargsyan A, Sarkisyan D and Adams C S 2012 *Phys. Rev. Lett.* **109** 233001
[43] Whittaker K A, Keaveney J, Hughes I G and Adams C S 2015 *Phys. Rev.* A **91** 032513
[44] Agnelli G, Cacciani A and Fofi M 1975 *Sol. Phys.* **44** 509
[45] Cacciani A and Fofi M 1978 *Sol. Phys.* **59** 179
[46] Sorokin P P, Lankard J R, Moruzzi V L and Lurio A 1969 *Appl. Phys. Lett.* **15** 79
[47] Endo T, Yabuzaki T, Kitano M, Sato T and Ogawa T 1977 *IEEE J. Quantum Electron.* **13** 866
[48] Endo T, Yabuzaki T, Kitano M, Sato T and Ogawa T 1978 *IEEE. J. Quantum Electron.* **14** 977
[49] Dick D J and Shay T M 1991 *Opt. Lett.* **16** 867
[50] Menders J, Benson K, Bloom S H, Liu C S and Korevaar E 1991 *Opt. Lett.* **16** 846
[51] Popescu A, Schorstein K and Walther T 2004 *Appl. Phys.* B **79** 955
[52] Chen H, White M A, Krueger D A and She C Y 1996 *Opt. Lett.* **21** 1093
[53] Fricke-Begemann C, Alpers M and Höffner J 2002 *Opt. Lett.* **27** 1932
[54] Huang W, Chu X, Williams B P, Harrell S D, Wiig J and She C-Y 2009 *Opt. Lett.* **34** 199
[55] Harrell S D, She C Y, Yuan T, Krueger D A, Plane J M C and Slanger T 2010 *J. Atmos. Sol.-Terr. Phys.* **72** 1260
[56] Wanninger P, Valdez E C and Shay T M 1992 *IEEE Photonics Technol. Lett.* **4** 94
[57] Choi K, Menders J, Searcy P and Korevaar E 1993 *Opt. Commun.* **96** 240
[58] Miao X, Yin L, Zhuang W, Luo B, Dang A, Chen J and Guo H 2011 *Rev. Sci. Instrum.* **82** 086106
[59] Bloom S H, Kremer R, Searcy P A, Rivers M, Meders J and Korevaar E 1991 *Opt. Lett.* **16** 1794
[60] Bloom S H, Searcy P A, Choi K, Kremer R and Korevaar E 1993 *Opt. Lett.* **18** 244
[61] Junxiong T, Qingji W, Yimin L, Liang Z, Jianhua G, Jiankun K and Lemin Z 1995 *Appl. Opt.* **34** 2619
[62] Shan X, Sun X, Luo J, Tan Z and Zhan M 2006 *Appl. Phys. Lett.* **89** 191121
[63] Frey R and Flytzanis C 2000 *Opt. Lett.* **25** 838

[64] Abel R P, Krohn U, Siddons P, Hughes I G and Adams C S 2009 *Opt. Lett.* **34** 3071
[65] Siyushev P, Stein G, Wrachtrup J and Gerhardt I 2014 *Nature* **509** 66
[66] Zielińska J A, Beduini F A, Lucivero V G and Mitchell M W 2014 *Opt. Express* **22** 25307
[67] Kiefer W, Löw R, Wrachtrup J and Gerhardt I 2014 *Sci. Rep.* **4** 6552
[68] Zentile M A, Whiting D J, Keaveney J, Adams C S and Hughes I G 2015 *Opt. Lett.* **40** 2000
[69] Yin B and Shay T M 1991 *Opt. Lett.* **16** 1617
[70] Harrell S D, She C-Y, Yuan T, Krueger D A, Chen H, Chen S S and Hu Z L 2009 *J. Opt. Soc. Am.* B **26** 659
[71] Zielińska J A, Beduini F A, Godbout N and Mitchell M W 2012 *Opt. Lett.* **37** 524
[72] Budker D, Gawlik W, Kimball D F, Rochester S M, Yashchuck V V and Weis A 2002 *Rev. Mod. Phys.* **74** 1153
[73] Menders J, Searcy P, Roff K and Korevaar E 1992 *Opt. Lett.* **17** 1388
[74] Franke-Arnold S, Arndt M and Zeilinger A 2001 *J. Phys. B: At. Mol. Opt. Phys.* **34** 2527
[75] Alcock C B, Itkin V P and Horrigan M K 1984 *Can. Metall.* Q. **23** 309
[76] Zentile M A, Keaveney J, Weller L, Whiting D J, Adams C S and Hughes I G 2015 *Comput. Phys. Commun.* **189** 162
[77] Corney A 1977 *Atomic and Laser Spectroscopy* (Oxford: Oxford University Press) pp 1–763
[78] Jackson J D 1999 *Classical Electrodynamics* 3rd edn (New York: Wiley) pp 1–808
[79] Russell S and Norvig P 2003 *Artificial Intelligence: A Modern Approach* 2nd edn (New Jersey: Pearson Education Inc.) pp 1–1080
[80] Hughes I G and Hase T P A 2010 *Measurements and Their Uncertainties: A Practical Guide to Modern Error Analysis* 1st edn (Oxford: Oxford University Press) pp 1–136
[81] Nelder J A and Mead R 1965 *Comput. J.* **7** 308
[82] Barwood G P, Gill P and Rowley W R C 1991 *Appl. Phys.* B **53** 142
[83] Ye J, Swartz S, Jungner P and Hall J L 1996 *Opt. Lett.* **21** 1280
[84] Falke S, Tiemann E, Lisdat C, Schnatz H and Grosche G 2006 *Phys. Rev.* A **74** 032503
[85] Siddons P, Adams C S and Hughes I G 2009 *J. Phys. B.: At. Mol. Opt. Phys.* **42** 175004
[86] Smith D A and Hughes I G 2004 *Am. J. Phys.* **72** 631
[87] Sherlock B E and Hughes I G 2009 *Am. J. Phys.* **77** 111
[88] Siddons P, Adams C S, Ge C and Hughes I G 2008 *J. Phys. B.: At. Mol. Opt. Phys.* **41** 155004
[89] Rotondaro M D and Perram G P 1997 *J. Quant. Spectrosc. Radiat. Transfer* **57** 497
[90] Zameroski N D, Hager G D, Rudolph W, Erickson C J and Hostutler D A 2011 *J. Quant. Spectrosc. Radiat. Transfer* **112** 59
[91] Novikova I, Matsko A B and Welch G R 2002 *Appl. Phys. Lett.* **81** 193
[92] Wells N P, Driskell T U and Camparo J C 2014 *Phys. Rev.* A **89** 052516